Environmental Science: Atmospheres

ROYAL SOCIETY OF CHEMISTRY

PAPER

View Article Online
View Journal | View Issue

Cite this: *Environ. Sci.: Atmos.*, 2025, **5**, 690

Cl_2^- chemical ionization mass spectrometry (Cl_2-CIMS) for the measurement of acyl peroxy radicals†

Tyson C. Berg, Michael F. Link ‡ and Delphine K. Farmer *

Received 7th April 2025
Accepted 28th April 2025

DOI: 10.1039/d5ea00043b

rsc.li/esatmospheres

Organic peroxy radicals (RO_2) are produced in the atmosphere by oxidation of volatile organic compounds (VOCs) and, in some cases, VOC photolysis. However, photolytic sources of RO_2 are often poorly understood, in part due to challenges in directly detecting RO_2 in both ambient and laboratory settings. We investigated Cl_2^- as a chemical ionization mass spectrometry reagent ion (Cl_2-CIMS) for measuring and speciating RO_2 in a laboratory setting. Cl_2-CIMS was more sensitive to the acetyl peroxy radical ($CH_3C(O)O_2$; 2.30 ± 0.04 ncps/ppt) than iodide CIMS (I-CIMS; 1.54 ± 0.03 ncps/ppt), but high backgrounds in our setup resulted in a slightly higher detection limit of 5 ppt (1 second integration) for Cl_2-CIMS than I-CIMS (2 ppt). We demonstrate the application of Cl_2-CIMS by quantifying the quantum yields of two radical products, $CH_3C(O)$ and $C_2H_5C(O)$, from methyl ethyl ketone photolysis at 254 nm. We identified O_2^- and Cl^- as possible secondary reagent ions that created unintended product ions in our experiments and thus could complicate the interpretation of Cl_2-CIMS mass spectra for complex atmospheric samples. While several strategies may minimize these effects, Cl_2-CIMS is suitable for measuring RO_2 in controlled laboratory experiments.

Environmental significance

Organic peroxy radicals are intermediates in the atmospheric oxidation cycles of organic molecules which impact production of atmospheric free radicals and ozone. Speciated measurements of organic peroxy radicals in the atmosphere are difficult but possible through recent advancements in chemical ionization mass spectrometry. We developed a chemical ionization mass spectrometry method using Cl_2^- as the primary reagent ion for detection of select organic peroxy radicals. We demonstrate this technique through laboratory measurements of the acetyl and propionyl peroxy radical quantum yields from methyl ethyl ketone photolysis. Cl_2^- reagent ion CIMS may be applicable to ambient measurements of organic peroxy radicals, if methods are developed for better isolation of Cl_2^- chemistry from reactions of secondary reagent ions.

Introduction

Organic peroxy radicals (RO_2) are key components of atmospheric oxidation chemistry but are challenging to measure due to their high reactivity and low ambient concentrations ($\sum RO_2 \leq 40$ ppt).[1,2] RO_2 reactions control hydroxyl (OH) radical production and can contribute to radical termination reactions, thus influencing oxidative capacity of the atmosphere and impacting air quality.[3] RO_2 are primarily formed from the oxidation of volatile organic compounds, though certain moieties, such as aldehydes and ketones, can also undergo photolysis to produce RO_2.[4]

Approaches to measuring RO_2 are primarily spectroscopic, including ultraviolet[3] and infrared absorbance[5] measurements and cavity ring-down spectroscopy.[6] Laser-induced fluorescence measurements are possible following the conversion of RO_2 to OH through reaction with CO and NO.[7] Chemical amplification of RO_2 is also possible through reaction with CO and NO, or C_2H_6 and NO, to produce and measure NO_2.[8,9] However, these spectroscopic techniques typically cannot quantify speciated radicals and are often limited to measuring HO_2 in the lab[10] (HO_2 can be considered the smallest RO_2 species, given its analogous sources and sinks) or summed concentrations of many RO_2 in the field.[11]

There is a clear need for new analytical techniques to directly measure and speciate RO_2. Ambient measurements would be improved through the development of a method that could detect individual RO_2 species in the field. Ambient concentrations of RO_2 other than CH_3O_2 and HO_2 are typically a few ppt or less.[12]

Better RO_2 measurements would also improve laboratory data on RO_2 production from organic gas photolysis. Photolytic sources of RO_2 become more important relative to oxidation reactions in the upper troposphere where oxidants (OH, O_3, NO_3, Cl) are scarce and the actinic flux is higher compared to

Department of Chemistry, Colorado State University, Fort Collins, Colorado 80523, USA. E-mail: delphine.farmer@colostate.edu

† Electronic supplementary information (ESI) available. See DOI: https://doi.org/10.1039/d5ea00043b

‡ Now at Engineering Laboratory, National Institute of Standards and Technology, Gaithersburg, Maryland 20899, USA.

the rest of the troposphere. For example, acetone photolysis is thought to produce HO_x (OH and HO_2) at a similar rate to the $O(^1D) + H_2O$ reaction in the upper troposphere.[13,14] However, the role of acetone in upper tropospheric HO_x production is poorly understood, as laboratory studies of acetone photolysis quantum yields are limited to indirect measurements of the dominant products: acetyl peroxy ($CH_3C(O)O_2$) and methyl peroxy (CH_3O_2) radicals. This results in substantial uncertainties in acetone photolysis quantum yields.[15] Prior studies typically measure either minor photolysis product channels[16] or stable products (*e.g.*, CO, CO_2, and peroxyacetyl nitrate) of secondary reactions.[17–19] Photolysis quantum yields for larger and more complex ketones are even more limited, as few techniques can speciate $CH_3C(O)O_2$ and CH_3O_2 radicals from RO_2 of different structures with fast time resolution.[10]

One technique that can provide fast, direct, and speciated detection of RO_2 is chemical ionization mass spectrometry (CIMS). CIMS has been used to measure RO_2 in both laboratory and ambient settings. Direct CIMS detection methods include measurements of HO_2 with I^- (I-CIMS)[20] and Br^- reagent ions,[21,22] acyl peroxy radicals ($R(O)O_2$) and other RO_2 with I-CIMS,[23–26] and highly oxidized molecule RO_2 with NH_4^+, $CH_3C(O)O^-$,[27] or $C_3H_7NH_3^+$ reagent ions.[28] Additional derivatization-aided detection methods exist for H_3O^+, NH_4^+,[29] and NO_3^-, but are typically labor-intensive.[12,30] We recently described the use of I-CIMS to measure ketone photolysis product quantum yields *via* direct detection of $RC(O)O_2$ produced from photolysis of methyl ethyl ketone (MEK) and 2,3-butadione.[23]

However, available CIMS reagent ions, including iodide, are often subject to interferences that impact RO_2 detection such as decreases in sensitivity due to small amounts of water vapor,[22] unintended production of radicals inside the instrument,[21] and secondary ion chemistry that complicates quantification.[31] The sensitivities of CIMS reagent ions, such I^- and Br^-,[22,25] can be temperature dependent as well. Current detection limits for RO_2 at short integration times (~1 s) are often too high (>5 ppt) for ambient measurements. Laboratory measurements of ketone photodissociation quantum yields are also challenged by high detection limits. Investigation into alternate CIMS reagent ions to measure speciated RO_2 is warranted.

We describe a reagent ion system for CIMS with Cl_2^- as the primary reagent ion (Cl_2-CIMS). We investigate the ion-molecule chemistry and demonstrate the application of Cl_2-CIMS to measurements of $RC(O)O_2$ from photolysis of acetone and MEK at 254 nm. Through organic acid and woodsmoke sampling, we evaluate the potential and limitations of Cl_2-CIMS in ambient measurements.

Methods

The chemical ionization mass spectrometer

We used a time-of-flight chemical ionization mass spectrometer with atmospheric pressure interface (CIMS; Aerodyne Research, Inc.), which consists of a standard Aerodyne Research Inc. designed ion-molecule reaction region (IMR), ion optics, and a time-of-flight mass analyzer with a multi-channel plate detector.[32,33] In the IMR, sample air interacts with a flow of reagent ions, which ionize analyte molecules through clustering, proton transfer, charge transfer, or other reactions. We operated the CIMS with a typical IMR pressure of 65 mbar. The ion optics consist of one small quadrupole and one large quadrupole, plus multiple skimmers and a segment of ion lenses, operated at increasing voltage (in this case, increasing negative voltages) as sample air moves from the high-to low-pressure regions. These sections maximize ion transport through the instrument as the total pressure decreases to 1×10^{-6} mbar in the time-of-flight region. The time-of-flight mass analyzer had a mass resolution of 3500 m/Δm ($\Delta m = 0.04$ at m/z 144.95, the m/z for $Cl_2(CH_3C(O)O_2)^-$), adequate for determining the elemental composition of detected ions in the size range described here.

We introduced reagent ion flow through the ionizer port on the IMR (Fig. 1), with a sealed Po-210 α-particle source (Model P-2021; NRD, LLC) ion source. Cl_2-CIMS reagent ions were formed by flowing trace concentrations of Cl_2 through the ion source. We used 12 L glass bulbs filled to 1250 mbar with 100 to 400 ppm Cl_2 in ultra-high purity N_2 (99.999%; Airgas) and calibration gas cylinders containing 10 or 40 ppm Cl_2 in N_2 (Gasco) as the reagent Cl_2 sources. A critical orifice limited Cl_2 flows at 10 mL min^{-1} from the 12 L glass; flow from the Cl_2 cylinders was adjusted by a precision needle valve. We used N_2, mixtures of N_2 and O_2 (99.994%; Airgas), or ultra-zero air (UZA; 99.999%; Airgas) as carrier gases for the Cl_2 reagent mixture. Needle valves controlled total carrier gas flow at >1250 mL min^{-1}, which diluted Cl_2 mixing ratios to ≤ 1 ppm in the ionizer. Unless otherwise stated, we used ~100 ppb Cl_2 in UZA carrier gas for Cl_2-CIMS reagent ion generation.

For I-CIMS, we generated I^- by passing a constant flow of N_2 over a CH_3I permeation tube heated to 40 °C through the ionizer. The constant flow and temperature on the permeation tube were maintained when I-CIMS was not in use. We estimate CH_3I concentration at the ionizer to be on the order of 500 ppb. We controlled water vapor partial pressure in the IMR through an additional port by changing the ratio of dry and water-saturated N_2 while keeping total flow constant. The humidified line was typically maintained at 80% RH, providing ~0.5 mbar H_2O to the IMR.

Calibrations

We calibrated the Cl_2-CIMS for ozone (O_3), formic, acetic, propanoic, and isobutyric acids, and $CH_3C(O)O_2$. A calibrated O_3 source (Model 306, 2B Technologies) generated O_3 between 25-200 (±2.0%) ppb in a 1600 mL min^{-1} flow of air, which we diluted with UZA to 2 L min^{-1} before sampling by the Cl_2-CIMS. Custom permeation tubes containing liquid organic acids were held at 40 °C and served as the acid calibration source. The permeation tube emission rates were determined gravimetrically. We used a custom peroxyacetyl nitrate (PAN) source[34] for CIMS calibration to $CH_3C(O)O_2$. The PAN calibration source photolyzes acetone in UZA to form $CH_3C(O)O_2$ and CH_3O_2. These radicals then react with NO to form NO_2, $CH_3C(O)O$ and CH_3O. The NO_2 reacts with the remaining $CH_3C(O)O_2$. In the

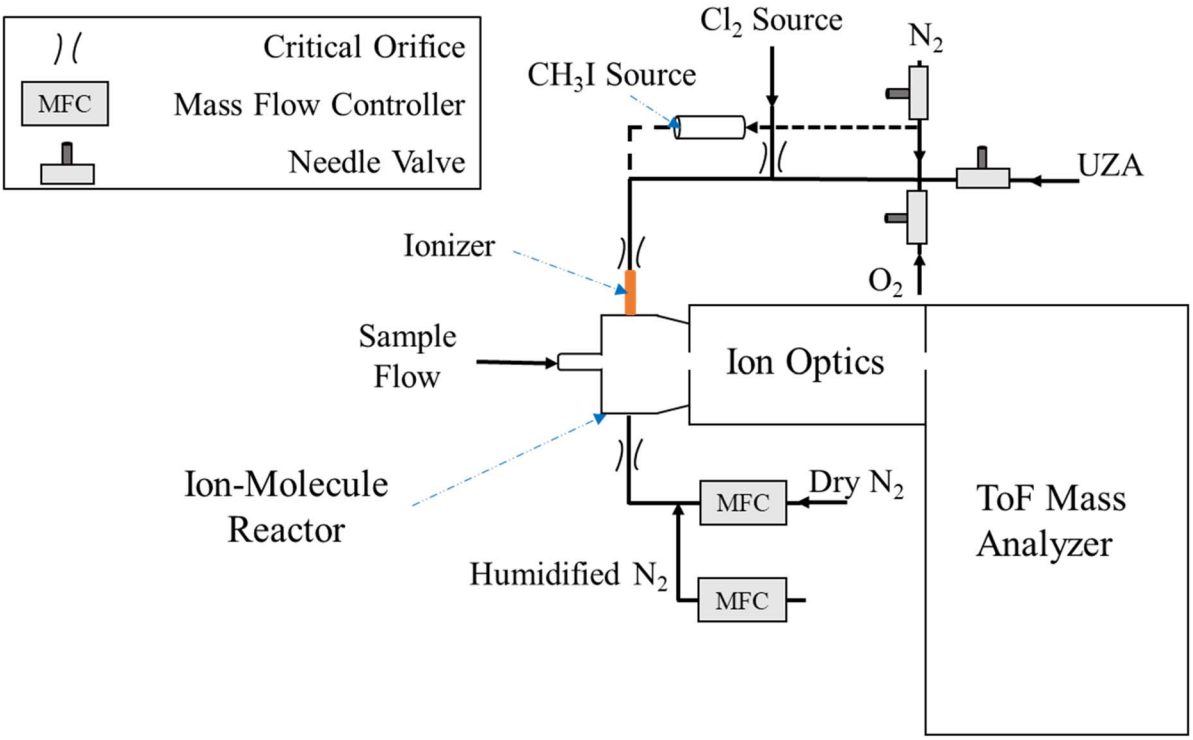

Fig. 1 Schematic of flows to introduce Cl_2^- reagent ions into the IMR of the CIMS. Describes the major CIMS components and the ionizer; flows of Cl_2, N_2, humidified N_2, zero air, and oxygen; and sample flow. The dashed lines and arrows denote the flow path used to produce I^- reagent ions from CH_3I in N_2. This path was not permanently attached to the Cl_2 flow system but replaced the Cl_2 flow through the ionizer during I-CIMS operation.

source we mixed a 60 mL min^{-1} flow of 18 ppm acetone in UZA (Scott-Marin) with 2 mL min^{-1} of 2 ppm NO in N_2. NO mixtures were prepared in 12 L glass bulbs. The light source was a phosphorus-coated Hg lamp (Jelight), with primary emission at 285 nm. Photolysis of the acetone-NO mixture occurred in a 200 cm^3 quartz cell at 1070 mbar and approximately room temperature, producing a 60 mL min^{-1} flow containing 40 ppb of PAN. The PAN concentration output of the device was calibrated by GC-ECD prior to our use. Further details on the custom PAN source are available in Flocke *et al.*[34] We diluted this PAN flow into 2 to 5 L min^{-1} N_2 and thermally decomposed PAN at 150 °C to produce $CH_3C(O)O_2$ mixing ratios from 0.48 to 0.96 ppb. A heating rope around a 0.25 in O.D. glass sampling tube 1 cm from the CIMS inlet provided the necessary heating for PAN thermal decomposition.[23] We calibrated the Cl_2-CIMS to analytes at a Cl_2 reagent mixture concentration of 100 ppb. Sensitivities are reported for IMR water partial pressure of 0.5 mbar and a total pressure of 65 mbar. All calibration standards were measured by the Cl_2-CIMS as a function of (i) Cl_2 ionizer concentrations (0.1 to 1.5 ppm), (ii) ion-molecule reactor (IMR) pressure between 50 and 100 mbar, (iii) IMR water partial pressure between 0 and 0.8 mbar, and (iv) de-clustering potential[35] between the front of the second quadrupole and the adjacent (up-flow) skimmer plate (Fig. S1†).

Sensitivities were calculated as the slope of the line of detected ion signal *versus* input concentration and reported as normalized ion counts per second per part per trillion (ncps/ppt; per 1×10^6 Hz of summed reagent ions). Unless indicated otherwise, Cl_2-CIMS signals are normalized to the sum of Cl^-, Cl_2^-, Cl_3^-, and O_2^-, the identified potential reagent ions. I-CIMS signals are normalized to the sum of I^- and $I(H_2O)^-$, the two primary reagent ions for this chemistry. Typical total reagent ion counts for both chemistries were between one and two million Hz. However, the reagent ion counts for Cl_2-CIMS varied, dependent on reagent gas O_2 content, and other instrument conditions as described in calibration tests (i)–(iv) above. All signals were normalized to total reagent ion counts, as described here, for comparisons across changing instrument conditions. Limits of detection (1 s integration) are calculated as three times the background signal-to-noise ratio and assuming a poisson distribution for background count rates.[23,32]

Ketone photolysis product quantum yields

To evaluate whether Cl_2^- was a better reagent ion for laboratory radical measurements, we compared measurements of $CH_3C(O)O_2$ and propionyl peroxy radicals ($C_2H_5C(O)O_2$), generated from photolysis of acetone and MEK, acquired with Cl_2-CIMS *versus* I-CIMS. In these experiments, ketone photolysis generated acyl peroxy radicals ((R1a) and (R1b)):

$$RC(O)CH_3 + h\nu \rightarrow RC(O) + CH_3 \quad \text{(R1a)}$$

$$RC(O) + O_2 + M \rightarrow RC(O)O_2 \quad \text{(R1b)}$$

We produced the MEK and acetone standards in 12 L glass bulbs containing percent-level ketone in N_2 taken from the

headspace of purified liquid ketones. Ketone samples in vacuum storage flasks were purified by freezing the liquid and pumping out the headspace. Ketone bulb concentration was determined through absorbance of 254 nm light (Hg Pen-Ray lamp; Analytik Jena) in a 50 cm glass cell with quartz end windows. We measured absorbance by bulb contents relative to background intensity in dry N_2 in triplicate, using a lab-built photodiode detector.

The photolysis reactor was a 1 in O.D. glass tube with three 0.25 in O.D. ports for the addition of photolyte mixture and sampling by the CIMS and exhaust. A Hg Pen-Ray 254 nm lamp was inserted 3 in into the reactor in a 0.5 in O.D. quartz test tube. The CIMS sampled from the photolysis reactor 1 cm from the end of the Pen-Ray lamp through an inserted 0.25 in glass tube.

During photolysis experiments, 10 mL min^{-1} of ketone in N_2 was mixed with 7 L min^{-1} of 21% O_2 in N_2 before entering the reactor adjacent to the Pen-Ray lamp housing. We measured the background flow of O_2 and N_2 before turning on the Pen-Ray Lamp for 100 s and then adding the ketone. After sampling during ketone photolysis for 5 min, we turned off the lamp, turned off the ketone flow, and sampled for at least one minute before turning the lamp on again. Experiments were run with both acetone and MEK. The Cl_2-CIMS detected $CH_3C(O)O_2$ primarily as the cluster $Cl_2(CH_3C(O)O_2)^-$ (R2):

$$CH_3C(O)O_2 + Cl_2^- \rightarrow Cl_2(CH_3C(O)O_2)^- \quad (R2)$$

By maintaining constant photolysis reactor conditions over the course of the experiment, we determined MEK photolysis product quantum yields from the ratio of $Cl_2(RC(O)O_2)^-$ signals between the two photolysis steps without needing to consider the reaction time of photon flux components of the photolysis rate coefficient eqn (E1).[23]

$$\Phi_{254}^{MEK,RC(O)O_2} = \frac{S_{Cl_2(CH_3C(O)O_2)^-}[\text{acetone}]\sigma_{254}^{\text{acetone}}\Phi_{254}^{Ac,CH_3C(O)}}{S_{Cl_2(RC(O)O_2)^-}[\text{MEK}]\sigma_{254}^{\text{MEK}}} \quad (E1)$$

where S represents the Cl_2-acylperoxy radical cluster ion signals produced during photolysis steps (Hz), σ and φ are the terms for ketone 254 nm absorption cross section and RC(O) photolysis product quantum yield, respectively, and [acetone] and [MEK] are ketone concentrations in the photolysis reactor. Details on experiments performed to ensure negligible impact of radical–radical and wall loss reactions on $RC(O)O_2$ yields with this reactor and experimental design are described by Link *et al.*[23]

Woodsmoke experiments

The Cl_2-CIMS sampled woodsmoke from a 1 m^3 Teflon chamber that had ports for air sampling, injection of smoke, and a constant flow of 3 L min^{-1} zero air (produced by zero air generator; Model 7000, Environics). Following the method described in Li *et al.*,[36] we burned ~1 g of Douglas fir woodchips in a Breville (BSM600SILUSC) cocktail smoker and injected the smoke directly into the chamber. This injection produced approximately 300 μg m^{-3} of smoke aerosol along with concentrated gases that could be analyzed by the CIMS. We connected the CIMS to a sampling port through ~1 m of PFA tubing (0.25 in O.D.) with a PTFE filter to remove particles. No lights were used to induce chemical aging of the smoke. A manual three-way valve allowed zero air to bypass the chamber directly to the CIMS. During measurements, we first flowed only zero air into the chamber for a background measurement before injecting smoke. The Cl_2-CIMS sampled smoke from the chamber for 2 hours. We then switched to I-CIMS mode and performed the same woodsmoke experiment with a new smoke addition. For analysis of woodsmoke samples, we identified ions that increased during smoke sampling with m/z < 300 for Cl_2-CIMS and < 350 for I-CIMS. We used a larger mass range for I-CIMS due to the difference in m/z of cluster ions formed with Cl_2^- and I^-. Thus, we account for approximately the same range of analyte masses with both reagent ion chemistries.

Results and discussion

Analyte detection

The Cl_2-CIMS produced ions through a variety of mechanisms including proton abstraction; adduct formation with Cl^-, Cl_2^-, and O_2^-; charge transfer; and secondary chemistry (Table 1 and Fig. S2†). Little fragmentation was observed. The dominant product ion varied by analyte. Cl_2^- cluster ions provided the largest sensitivity for formic acid and $CH_3C(O)O_2$, while product ions from secondary chemistry and O_2^- clustering provided the largest sensitivities for O_3 and C_2–C_4 organic acids, respectively. CO_3^- is a known product ion of O_3 for O_2-CIMS and is formed from the reaction of O_3^- with CO_2.[37] Though C_2–C_4 organic acids were detected as O_2^- clusters with sensitivities on the order of 1 to 2 ncps/ppt, Cl_2^- clusters produced much lower sensitivities at <0.02 ncps/ppt. C_2–C_4 organic acid clusters with Cl^- showed larger sensitivity than Cl_2^- at 1.2 ± 0.2 ncps/ppt for acetic acid, 0.215 ± 0.002 ncps/ppt for propanoic acid, and 0.142 ± 0.005 ncps/ppt for isobutyric acid.

Sensitivities to all analytes were independent of IMR pressure within the range of 50-100 mbar (Fig. S3†) but did vary with IMR water partial pressure (0-0.6 mbar; Fig. S4 and S5†), and declustering voltage (Fig. S6†). The largest water partial pressure impacts were observed for Cl^- and Cl_2^- clusters. Thus, we operated the Cl_2-CIMS optimized for $Cl_2(RC(O)O_2)^-$ (~0.5 mbar H_2O) and overall cluster ions production (dV = 1.4).

Sensitivity to $CH_3C(O)O_2$, detected as $Cl_2(CH_3C(O)O_2)^-$, was 2.30 ± 0.04 ncps/ppt when normalized to the total reagent ion signal, and 3.19 ± 0.05 ncps/ppt when normalized to the Cl_2^- reagent ion signal. In contrast to other analytes, alternate ion formation pathways were negligible for the acetyl peroxy radical. The sensitivity of Cl_2-CIMS was higher than that for I-CIMS (1.54 ± 0.03 ncps/ppt for $ICH_3C(O)O_2^-$) under the same measurement conditions. However, the LOD for I-CIMS was lower (2 ppt) than we obtained for Cl_2-CIMS (5 ppt) due to larger backgrounds for Cl_2-CIMS.

We note that CIMS users employ various normalization techniques; either normalizing data to total ion counts to account for slight variations in instrument performance, or normalizing data to the relevant reagent ion signals acknowledging that variations in just those signals can modulate the

Table 1 Analyte product ion detection and sensitivities

Analyte	Molecular formula	Product ions	Primary product ion	Primary ion sens. (ncps/ppt)[a]	LOD (ppt)	Calibration range (ppb)
Acetyl peroxy radical	$CH_3C(O)O_2$	$Cl_2CH_3C(O)O_2^-$	$Cl_2CH_3C(O)O_2^-$	2.30 ± 0.04 3.19 ± 0.05[b]	5	0.48–0.96
Ozone	O_3	O_3^-, CO_3^-	CO_3^-	0.78 ± 0.02	291	18.4–147
Formic acid	HC(O)OH	$ClRC(O)OH^-$,	$Cl_2HC(O)OH^-$	1.01 ± 0.02	73	33–65
Acetic acid	$CH_3C(O)OH$	$Cl_2RC(O)OH^-$,	$O_2CH_3C(O)OH^-$	1.6 ± 0.2	50	23–46
Propanoic acid	$C_2H_5C(O)OH$	$O_2RC(O)OH^-$, $RC(O)O^-$[c]	$O_2C_2H_5C(O)OH^-$	2.00 ± 0.01	9	8.7–17.2
Isobutyric acid	$C_3H_7C(O)OH$		$O_2C_3H_7C(O)OH^-$	1.11 ± 0.01	22	0.97–1.9

[a] Sensitivities normalized (per million ions) to sum of reagent ion signal (O_2^- + Cl^- + Cl_2^- + Cl_3^-). [b] Sensitivity normalized (per million ions) to Cl_2^- signal. [c] General formulas of observed product ions for all organic acids.

sensitivity to an analyte.[25,38,39] Different approaches to normalization impact the calculated sensitivity and detection limit. For example, we add a second Cl_2-CIMS sensitivity to $CH_3C(O)O_2$ (normalized to the Cl_2^- counts only) in Table 1 and Fig. S7,† due to a consistent relationship between Cl_2^- and $Cl_2(CH_3C(O)O_2)^-$ observed during $CH_3C(O)O_2$ calibration and MEK photolysis (Fig. S8†). This normalization method increased the normalized sensitivity, but the total sensitivity observed during the test remains the same. The Cl_2-normalized sensitivity serves as both the maximum possible sensitivity in a reagent ion spectrum of entirely Cl_2^- and the most accurate method of calculating sensitivity to $CH_3C(O)O_2$ between tests. The $CH_3C(O)O_2$ sensitivity normalized to the sum of Cl^-, Cl_2^-, Cl_3^-, and O_2^- did not

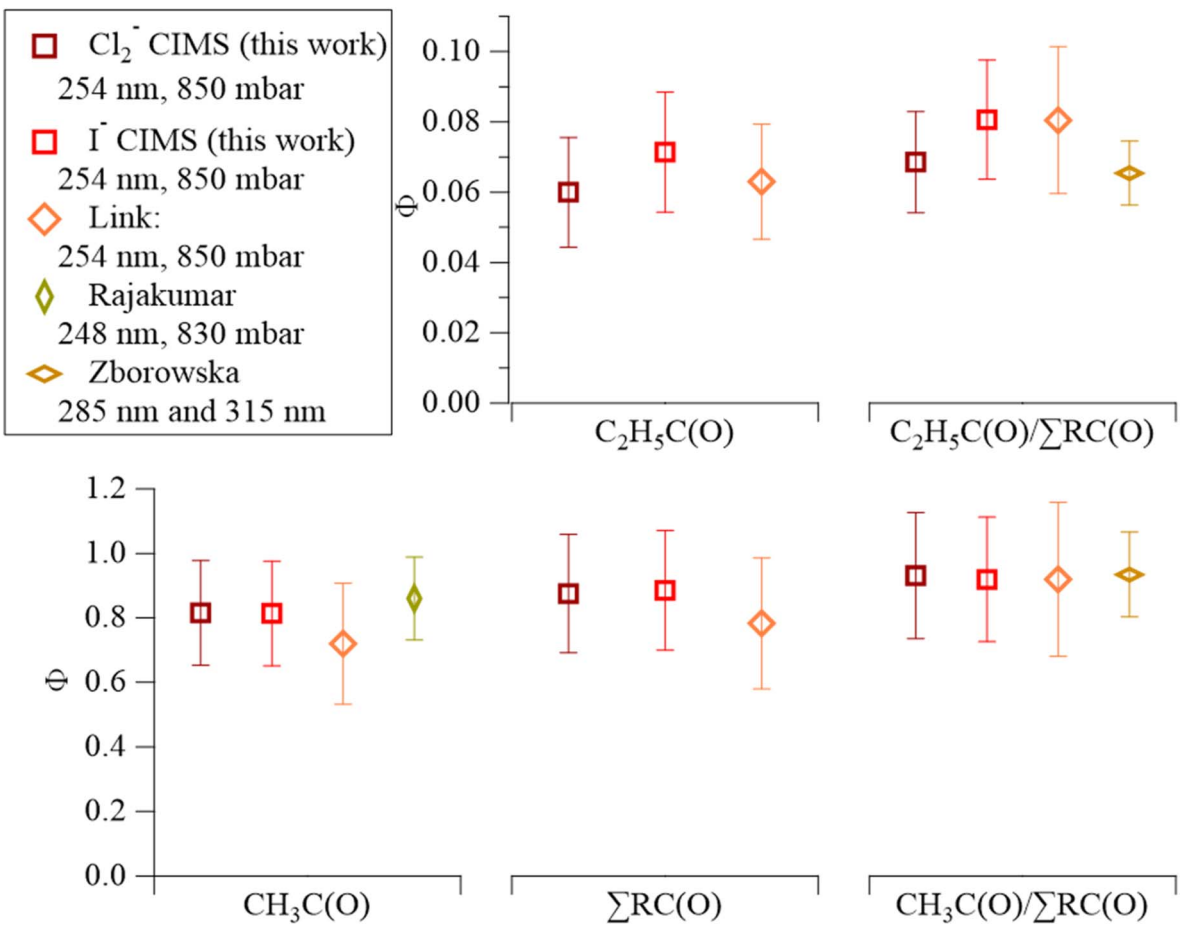

Fig. 2 Comparison of MEK photolysis product quantum yield values from the Cl_2-CIMS (dark red) and I-CIMS (light red) from this study to recent literature values. The *x*-axis consists of segments for each MEK photolysis product: $CH_3C(O)$ on the bottom-left, $C_2H_5C(O)$ on top-center, ΣRC(O) on the bottom-center, and branching ratios on the right ($C_2H_5C(O)/\sum RC(O)$ top; ($CH_3C(O)/\sum RC(O)$ bottom) orange diamonds represent values from Link *et al.*;[23] gold diamond represents the Rajakumar *et al.*[40] value for $\Phi_{CH_3C(O)}$; light-brown diamonds represent branching ratios derived from $C_2H_5C(O)$: $CH_3C(O)$ signal ratios in Zborowska *et al.*[19] Error bars represent experimental uncertainties.

reflect the difference of signal observed between Cl_2-and I-CIMS during MEK photolysis.

MEK photolysis product quantum yield measurements at 254 nm

The Cl_2-CIMS detected both $CH_3C(O)O_2$ and $C_2H_5C(O)O_2$ from MEK photolysis as clusters with Cl_2^-. We assume that the Cl_2-CIMS sensitivity to $CH_3C(O)O_2$ and $C_2H_5C(O)O_2$ are equivalent based on voltage scanning data. Briefly, by changing the voltage difference between two components in the ion-focusing regions of the CIMS, we provide adequate energy to de-cluster reagent ion-analyte adducts.[35,41] The voltage difference that corresponds to a 50% loss in adduct ion signal (dV50) correlates to the sensitivity of the instrument to the clustering mechanism.[42] The voltage scan provides a dV50 of 4.58 ± 0.05 V for $Cl_2(CH_3C(O)O_2)^-$ and 4.21 ± 0.05 V for $Cl_2(C_2H_5C(O)O_2)^-$ (Fig. S9†). This is quite close to the 0.3 V difference in dV50 found with I-CIMS,[23] indicating that the sensitivities of Cl_2-CIMS to $CH_3C(O)O_2$ and $C_2H_5C(O)O_2$ are similar. This assumption is further supported by the agreement of quantum yields between Cl_2-CIMS and I-CIMS and with prior literature.[19,40]

Cl_2-CIMS derived MEK photolysis quantum yields at 254 nm ($\Phi_{254}^{MEK,\ RC(O)}$) were consistent with previous measurements[19,23,40] and with I-CIMS $\Phi_{254}^{MEK,\ RC(O)}$ obtained as part of this work. $\Phi_{254}^{MEK,\ CH_3C(O)}$ and $\Sigma\Phi_{254}^{MEK,\ RC(O)}$ from Cl_2-CIMS and I-CIMS (Fig. 2) agreed within the measurement precision of 3%, while $\Phi_{254}^{MEK,\ C_2H_5C(O)}$ agreed within the experimental uncertainties of 26% and 24% calculated for Cl_2-CIMS and I-CIMS, respectively. The experimental uncertainties were 20% for $\Phi_{254}^{MEK,\ CH_3C(O)}$ and 21% for $\Sigma\Phi_{254}^{MEK,\ RC(O)}$ for both Cl_2-CIMS and I-CIMS. Signals for $Cl_2(CH_3C(O)O_2)^-$ and $Cl_2(C_2H_5C(O)O_2)^-$ obtained by Cl_2-CIMS during MEK photolysis were larger than the corresponding I^- cluster signals from I-CIMS (Fig. S8†). Cl_2-CIMS measured radical signals normalized to only Cl_2^- were a factor of 2.1 ± 0.1 larger than I-CIMS (normalized to the sum of I^- and $I(H_2O)^-$), in agreement with the sensitivity ratio (2.07 ± 0.05) obtained during calibrations. This indicates that the Cl_2-CIMS sensitivity to $RC(O)O_2$ was dependent on Cl_2^- and not related to the total reagent ion count.

Cl_2-CIMS reagent ion chemistry

Cl_2-CIMS reagent ion chemistry is a complex system of ionizing reactions involving Cl^-, Cl_2^-, Cl_3^-, and O_2^-, which is best

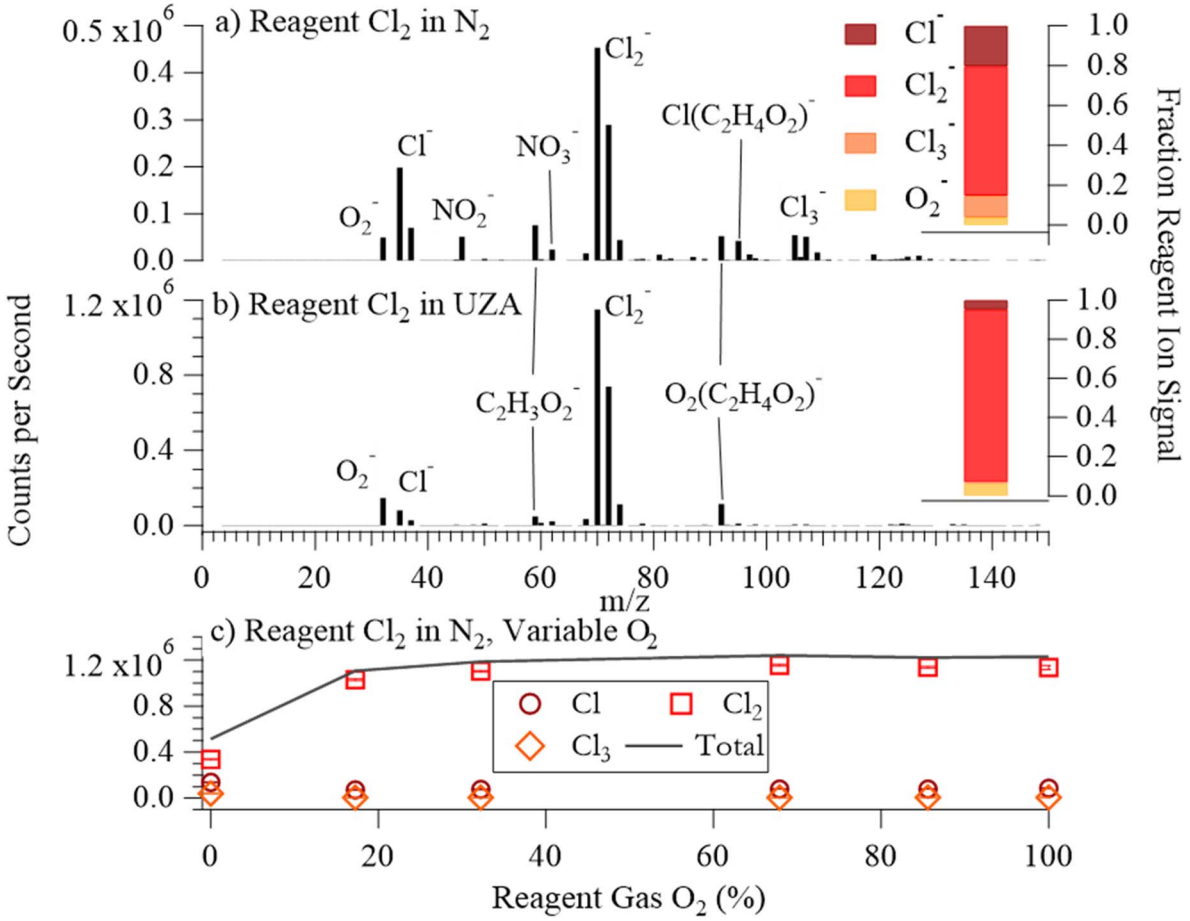

Fig. 3 (a) Mass spectrum for dry N_2 with a reagent ion flow of Cl_2 in N_2; fractional contributions of reagent ions (dark red: Cl^-, light red: Cl_2^-, orange: Cl_3^-, yellow: O_2^-) to total reagent ion counts in the right-hand inset. (b) Mass spectrum for dry N_2 with reagent ion flow of Cl_2 in UZA and the respective fractional reagent ion contribution inset. (c) Ion counts for Cl^-, Cl_2^- and Cl_3^- as a function of O_2 mixing ratio (%) in the reagent gas mixture (dry N_2 sampling). The black line represents the sum of these three ions.

described by first examining the ion chemistry of Cl_2 in N_2. In a reagent gas mixture with dry N_2, collisions of α-particles from the Po-210 source with N_2 produce free electrons[43] (R3a). Cl_2 is the primary molecule that attaches free electrons within the ionizer flow (R3b).

$$\alpha + N_2 \rightarrow N_2^+ + e^- + \alpha \quad \text{(R3a)}$$

$$e^- + Cl_2 \rightarrow Cl_2^-* \quad \text{(R3b)}$$

Excited Cl_2^-* formed by electron attachment can decompose to Cl^- and Cl (R4a),[44] though the example reagent ion spectrum in N_2 (Fig. 3(a)) shows a significant portion of Cl_2^-* in our system is stabilized by collisions (R4b). Cl_2^-* is the source of both Cl^- and Cl_2^- in the reagent ion spectra through either decomposition or collisional stabilization.

$$Cl_2^-* \rightarrow Cl + Cl^- \quad \text{(R4a)}$$

$$Cl_2^-* + M \rightarrow Cl_2^- + M* \quad \text{(R4b)}$$

$$Cl + Cl^- + M \rightarrow Cl_2^- \quad \text{(R5)}$$

The recombination reaction (R5) is a significant source of Cl_2^- for liquid phase studies but is not expected to be important here.[45] Instead, Cl^- can go on to react with Cl_2, forming the observed Cl_3^- signal (R6a), with $Cl_2^- + Cl_2$ (R6b) and $Cl_2^- + Cl$ (R6c) reactions also being possible sources of Cl_3^-.[46]

$$Cl^- + Cl_2 \rightarrow Cl_3^- \quad \text{(R6a)}$$

$$Cl_2^- + Cl \rightarrow Cl_3^- \quad \text{(R6b)}$$

$$Cl_2^- + Cl_2 \rightarrow Cl_3^- + Cl \quad \text{(R6c)}$$

We found an upper limit of 400 ppb Cl_2 in the reagent ion flow (Fig. 4(c)), above which point the Cl_2^- signal stopped increasing and Cl_3^- became the largest reagent ion signal. We were unable to isolate production of Cl_2^- through modulation of Cl_2 concentration in N_2 alone.

Impacts of O_2 and Cl_2 concentrations

The reagent ion distribution changed with the addition of O_2 (Fig. 3b and c). Adding ~21% O_2 to the ionizer flow increased total ion counts by 58%, increased the fraction of Cl_2^- ions in the total reagent ion signal from 60 to 90%, reduced Cl^- and Cl_3^- signals, and increased O_2^-. Due to the direct dependence of $Cl_2(RC(O)O_2)^-$ on Cl_2^-, the net result of these changes was a factor of 2.4 increase in total sensitivity to $RC(O)O_2$. Addition of O_2 also caused a 32% decrease of non-reagent ions in background mass spectra (Fig. 3a and b), leading to overall improvements in LODs.

The differences we observed in the reagent ion spectrum upon addition of O_2 result from a change in the primary Cl_2 ionization mechanism. At percent-level concentrations in the reagent gas mixture, O_2 becomes the primary electron capturing molecule (R7).

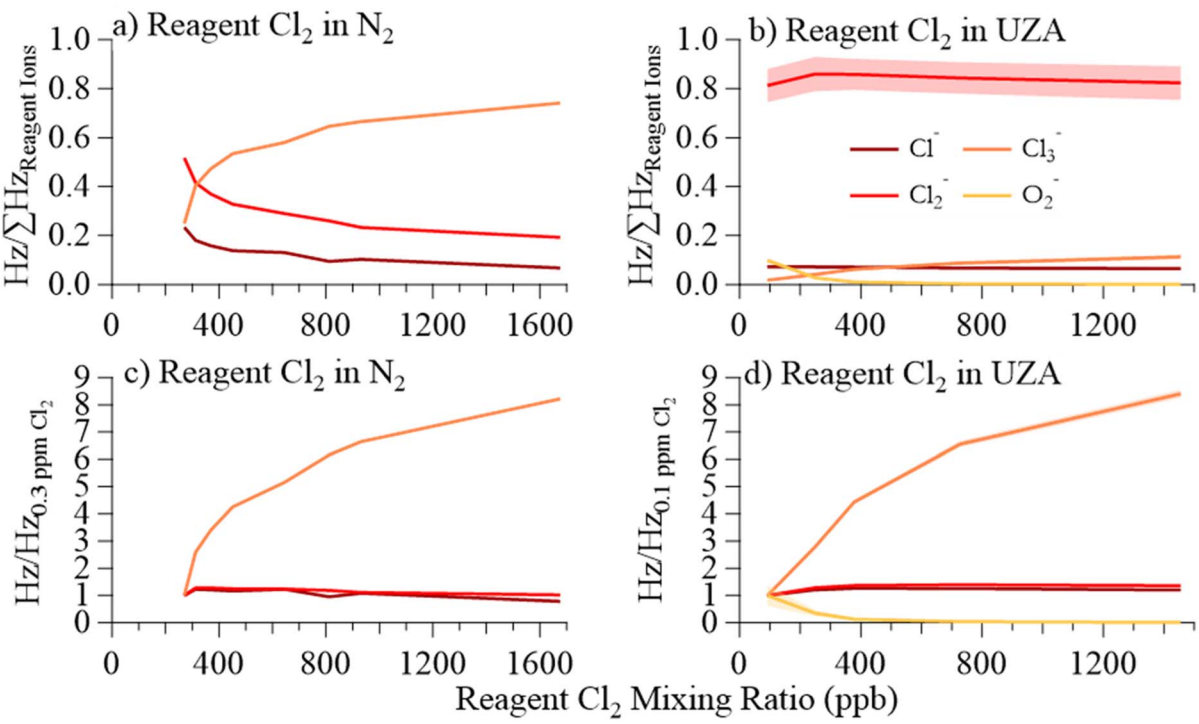

Fig. 4 (a) Fraction of total reagent ion signal for Cl^- (dark red), Cl_2^- (light red), and Cl_3^- (orange), as a function of reagent gas Cl_2 mixing ratio (ppb) in N_2. (b) Fraction of total reagent ion counts for Cl^-, Cl_2^-, and Cl_3^-, and O_2^- (yellow) as a function of reagent gas Cl_2 mixing ratio in UZA. (c) Reagent ion signal, relative to 300 ppb Cl_2, as a function of reagent gas Cl_2 mixing ratio in N_2. (d) Reagent ion signal, relative to 100 ppb Cl_2, as a function of reagent gas Cl_2 mixing ratio in UZA. All reagent ion data was collected while sampling dry N_2 to the CIMS inlet.

$$e^- + O_2 \rightarrow O_2^- \quad \text{(R7)}$$

Cl_2^- is a known product of Cl_2 ionization by O_2-CIMS,[47] and we hypothesize Cl_2^- is primarily formed here in a multiple step process. Electrons formed by ionization in the Po-210 source may predominately attach to O_2 molecules present in the reagent gas mixture at atmospheric mixing ratios. The electron affinities of Cl_2 and O_2 are 2.38 eV[48] and 0.451 eV,[49] respectively, indicating the following favorable electron transfer reaction as the primary source of Cl_2^- with O_2 in the reagent gas mixture (R8).

$$O_2^- + Cl_2 \rightarrow O_2 + Cl_2^- \quad \text{(R8)}$$

The reagent ion distribution impacts the chemical ionization mechanisms and thus sensitivity. We found that modulation of Cl_2 reagent gas concentration in UZA produced a negative correlation between Cl_2^- and O_2^- (Fig. 4(d)). Analyte ions for the organic acids, O_3, and $CH_3C(O)O_2$ responded to either Cl_2^- or O_2^-, depending on which ion chemistry produced each ion. The sensitivity of these analyte ions to changes in the Cl_2 mixing ratio in the reagent gas mixture (in UZA) are shown in Fig. 5, with the slopes and r^2 of the linear least squares fits in Table S10.† Cl^- and Cl_2^- signals correlated well to both the Cl^- and Cl_2^- cluster analyte ions ($r^2 > 0.73$ for Cl^- and > 0.59 for Cl_2^-). The exceptions were $Cl_2(C_2H_5C(O)OH)^-$, which had low sensitivity, and $Cl_2(CH_3C(O)O_2)^-$ at Cl_2 concentrations above 400 ppb (Fig. S11†). For Cl_2 reagent gas concentrations below 400 ppb, Cl_2^- correlated to $Cl_2(CH_3C(O)O_2)^-$ with slope = 0.53 and r^2 = 0.99. Fitting of O_2^- cluster and H^+ abstraction ion signals to Cl^- and Cl_2^- resulted in negative slopes for all sampled acids. We also observed negative Cl^- and Cl_2^- correlations for O_3^- and CO_3^- from O_3 and for $CH_3C(O)O^-$ and $CH_3C(O)O_2^-$ detected during $CH_3C(O)O_2$ sampling. The O_2^- clusters and H^+

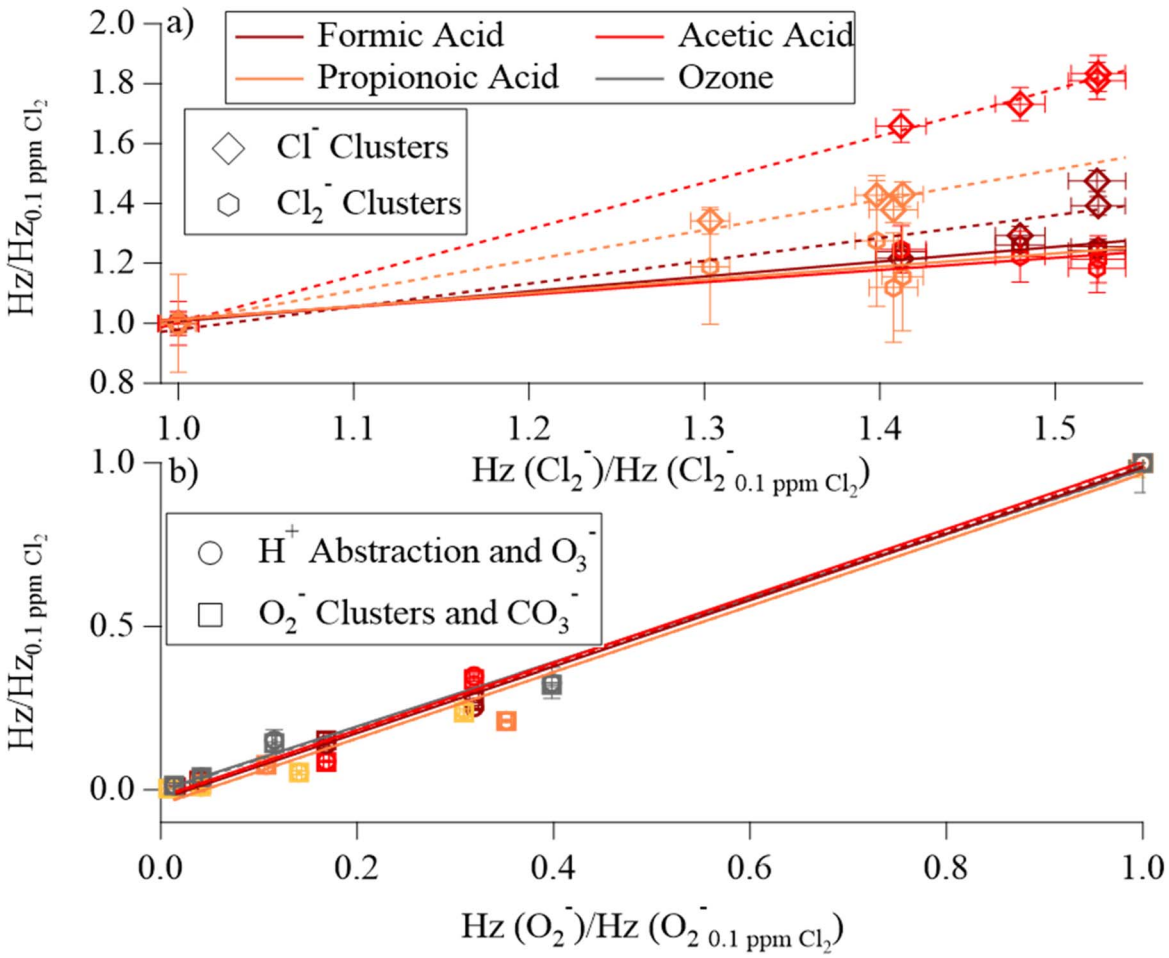

Fig. 5 (a) Correlation plot of Cl^- (diamonds) and Cl_2^- (hexagons) cluster ion signals for formic (dark red), acetic (light red), and propionic (orange) acids against background signals of Cl_2^- over the Cl_2 concentration changes. Linear correlation fits shown with dashed (Cl^- clusters) and solid (Cl_2^- clusters) lines. (b) Correlation plot of proton abstraction (circle) and O_2^- cluster (square) ion signals against background signals of O_2^- over the Cl_2 concentration changes. Acid signals are indicated by the same colors as (a), with gray markers for O_3 product ion correlations (squares for CO_3^- and circles for O_3^-). Linear fits are shown as dashed lines for proton abstraction and solid lines for O_2^- cluster. The *y*-axis represents ratios of the observed signal to the signal at the lowest Cl_2 concentration; all error bars represent propagated uncertainty of one standard deviation in signal at each Cl_2 concentration step. Isobutyric acid is left off to reduce graph clutter, as these signals had large uncertainty for Cl_2^- reactions. Fit information for isobutyric acid is provided in Table S10 and Fig. S12.†

abstraction products, instead, correlated strongly to O_2^- signal, as did O_3^-, CO_3^-, and $CH_3C(O)O_2^-$ ($r^2 > 0.96$; slopes = 1.0). Changes in Cl_3^- signal did not correlate to any analyte ion, returning slopes between 0.09 and −0.15.

The formation of Cl^- clusters from Cl^- ionization is straightforward. However, Cl^- cluster formation from Cl_2^- is also possible, due to the instability Cl_2^-. Here, the reaction between Cl_2^- and an analyte would act more like a ligand exchange, producing Cl-analyte ion and a Cl atom (R9).

$$Cl_2^- + RC(O)OH \rightarrow Cl + (RC(O)OH)Cl^- \quad (R9)$$

A similar ionization mechanism occurs with SF_6^- for some analytes.[50] Cl_3^- formation acts as a sink of sensitivity in the Cl_2-CIMS, as Cl_3^- signal did not show a positive correlation with any analyte ion. Cl_3^- is a cluster ion of Cl_2 and Cl^-, which has a high binding energy.[51] This binding energy was larger than that of the acid-Cl^- clusters (Fig. S6†). In addition, Cl_3^- has an electron affinity ≥ 3.8 eV,[46] making electron transfer ionization unfavorable for most analytes.

The results in Fig. 5 demonstrate that analyte ion production is directly dependent on the availability of reagent ions that produce each analyte ion, and not necessarily on total reagent ion count. This observation suggests that the proper normalization for analyte sensitivities is to the corresponding reagent ion, as we provide for $CH_3C(O)O_2$ in Table 1. Sensitivities for all organic acid and O_3 product ions are in Table S13.† Under the optimized conditions for Cl_2^- production in our system, the sensitivities normalized to Cl^- and Cl_2^- shift only slightly in Table S13† from those in Table 1, as Cl_2^- accounted for ≥ 80% of total reagent ion counts across these experiments and the sum of Cl^- and Cl_2^- accounted for ≥ 90%. Normalization to O_2^- increases the Cl_2-CIMS sensitivity to proton abstraction and O_2^- cluster products by at least an order of magnitude compared to Table 1. The O_2^- normalized sensitivities are near the collision limit, but sensitivities to $O_2(CH_3C(O)OH)^-$ and CO_3^- are much larger than that limit and thus imply that additional ionization mechanisms or interferences are occurring.

O_2^- normalized sensitivities of 98 ± 12 ncps/ppt for $O_2(CH_3C(O)OH)^-$ and 56 ± 4 ncps/ppt for CO_3^- suggest that the measured O_2^- signals may not be representative of the O_2^- concentrations in the IMR. These inflated sensitivities may be due to changes in transmission efficiency with mass, as CIMS of similar design have lower transmission efficiencies at low m/z.[52] If the reaction of O_2^- with Cl_2 does not run to completion before sample introduction, analyte ions will appear at signals consistent with a larger O_2^- concentration than was measured, also explaining the surprisingly high O_2^- normalized sensitivities. Despite this problem, sensitivities in Table S13† may provide more consistent comparison of Cl_2-CIMS response

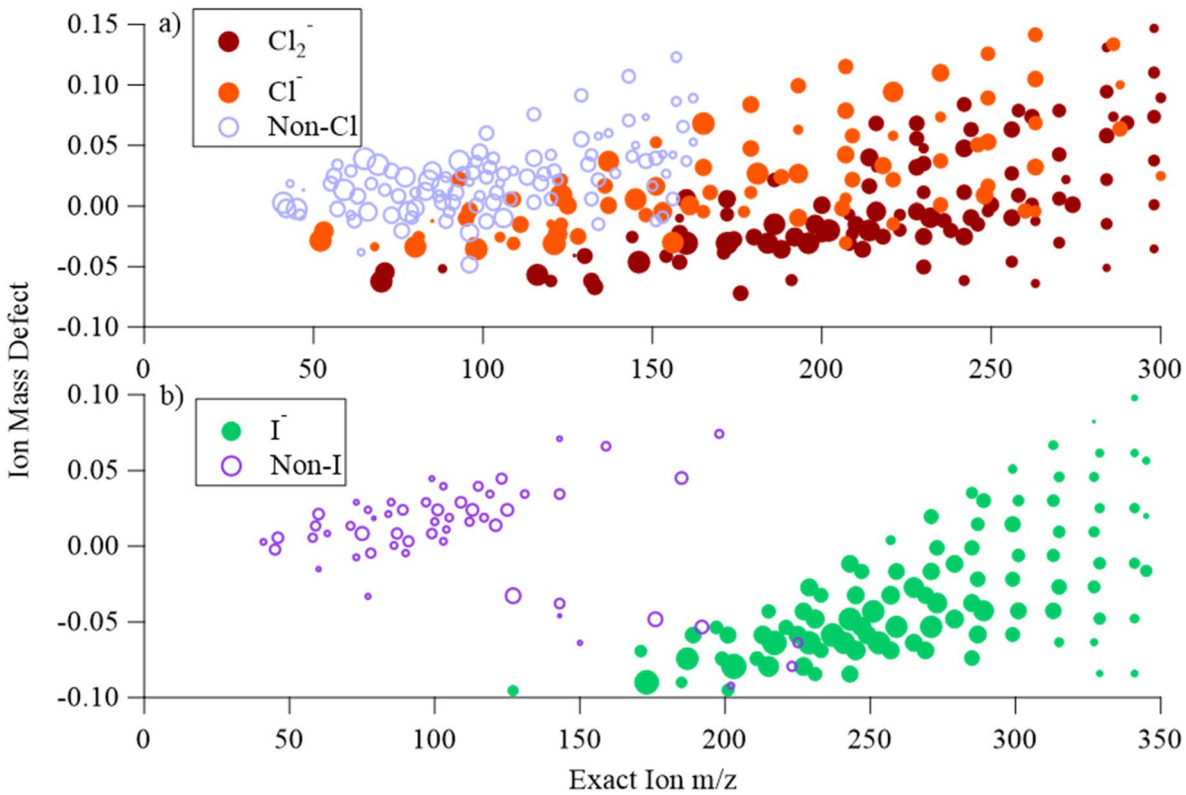

Fig. 6 (a) Mass defect plot for identified ions from woodsmoke sampling with Cl_2-CIMS. Blue circles indicate O_2^- cluster and non-clustered product ions, orange indicates Cl-containing, and red indicates Cl_2-containing formulas. (b) Mass defect plot for detected ions during I-CIMS sampling of woodsmoke. Purple circles indicate peaks that did not contain iodide while green indicates I-containing formulas. Dot size represents the relative signal increase between background and smoke sampling steps.

across changing instrument and sample conditions, as was the case for our $CH_3C(O)O_2$ calibration and MEK photolysis measurements.

Woodsmoke

While Cl_2-CIMS is an effective detection technique for RO_2 in controlled laboratory systems, woodsmoke demonstrates the problems of using Cl_2-CIMS for complex mixtures. We use ion mass defects (defined as the difference between the exact m/z of an ion and the nearest unit mass) to visualize the differences in ions that appear in the Cl_2-CIMS and I-CIMS mass spectra during woodsmoke experiments. Multiple reagent ions and potential reaction pathways produced more analyte ions with Cl_2-CIMS (>300 ions; Fig. 6(a)). The I-CIMS spectra contained about half as many ions, which were mostly produced from iodide adduct formation (177 ions; Fig. 6(b)). Though more peaks appeared for Cl_2-CIMS, these were not indicative of compounds unique to Cl_2-CIMS detection. Instead, the larger peak count in Cl_2-CIMS is a byproduct of multiple reagent ion chemistries, where a single analyte formula would appear in up to four product ions. We fit 103 Cl_2^- cluster analyte ions, which represented 39.8% of analyte ion signals measured with Cl_2-CIMS. 82 Cl^- clusters accounted for 21.6% of analyte ion signals, while 38.6% of analyte signal was from 128 ions which did not contain Cl. In contrast, the 111 identified I^- containing ions accounted for 99.8% of analyte signals measured with I-CIMS.

The largest signals for both reagent ions were small organic acids and peracids. Specifically, $C_2H_4O_2$, CH_2O_2 and $C_3H_6O_3$ were all measured at signals that were about two times greater than any other product by I-CIMS. These species were also among the most prominent Cl_2-CIMS signals. However, the highest analyte signal for Cl_2-CIMS was $O_2(CH_4O_2)^-$ (~200 000 cps), corresponding to the oxygen cluster for acetic acid. This observation again indicates that the conditions in the IMR do not reflect the final spectra, and that the Cl_2-CIMS acts largely as an O_2-CIMS under polluted sampling conditions.

The appearance of Cl_2^-, Cl^-, and O_2^- clusters, and molecular ions (or H^+ abstraction products) led to an array of possible mass defects. Overlap of ions at the same mass-to-charge occurred more frequently for Cl_2-CIMS. I-CIMS provided I^- clusters with large mass defects and a lack of competing ion-molecule reactions. Thus, ions detected by I-CIMS were more often separated from interfering peaks than those detected by Cl_2-CIMS. For example, nitrogen-containing products of biomass burning, including C_2H_5NO, CH_3NCO, C_3H_7NO,[53] could be identified with I-CIMS, but not clearly with Cl_2-CIMS. This limitation was largely due to the tendency for overlap of Cl_2^- (even mass) clusters, which might contain N, with Cl^- (odd mass) clusters, which did not (and *vice versa*). We saw little evidence for the identification of RO_2 in our data due to spectral complexity. It is also possible in a complex sample that side reactions of Cl_2-CIMS would produce ion formulas that are not representative of sampled molecular formulae, particularly if Cl radicals are formed from the decomposition of Cl_2^-. We could derive no clear evidence of this from the woodsmoke experiments but provide evidence of possible Cl radical impacts in Fig. S11.† Due to the detrimental complexities of the current Cl_2-CIMS ion chemistry, we could draw little else from the analysis of these smoke samples without significant alterations to the CIMS IMR design.

Conclusion

Direct measurements of RO_2 in both ambient and laboratory settings require low limits of detection (1 ppt). Cl_2-CIMS is an effective reagent ion chemistry for laboratory measurement of $CH_3C(O)O_2$ and $C_2H_5C(O)O_2$ with better sensitivity than existing I-CIMS measurements – capable of producing quantum yields for MEK photolysis consistent with results obtained from other measurement techniques in the literature. However, the reported LOD of 5 ppt, higher than that found for I-CIMS, is too high for ambient measurement of RO_2. The sensitivity of Cl_2-CIMS to $CH_3C(O)O_2$ and $C_2H_5C(O)O_2$ would be increased through isolation of Cl_2^- ionization chemistry, without the non-selective ionization of O_2^- or the potential for secondary chemistry of Cl atoms in the IMR. Such alterations to Cl_2-CIMS would lower LODs and expand its applications.

Reactions of O_2^- may be avoided by using a different electron donor. For the electron transfer with Cl_2 to occur, the electron donor must be more reactive than Cl_2^-. High purity air requires few considerations for use in CIMS reagent gas mixtures, compared to, for example, SF_6 (electron affinity = 1.05 eV).[50] In addition, O_2^- reacts with Cl_2 in our system to form Cl_2^- with few notable secondary products other than Cl^-. This is not a guarantee for other electron donors. A more effective means of isolating Cl_2^- chemistry may be to alter the IMR design to add an initial reaction chamber where the $O_2^- + Cl_2$ reaction would run to completion prior to sample introduction, thus minimizing O_2^- chemistry. However, such modifications were outside the scope of this study. With the current instrumental design, the multiple reagent ion chemistries present in the Cl_2-CIMS system prevent the reagent ion chemistry from being useful for ambient studies, as evidenced by the woodsmoke measurements. Alternatively, this work highlights the utility of dual reagent ions (Cl_2^- and O_2^-) to provide a selective measurement of acyl peroxy radicals.

Data availability

The data supporting this article have been included as part of the ESI.†

Conflicts of interest

The authors declare no conflicts of interest regarding the content of this manuscript.

Acknowledgements

We thank Dr Kathryn Mayer for assisting with the woodsmoke sampling tests. We thank Dr Frank Flocke for providing the PAN

source used for calibration tests. We thank the National Science Foundation (Grant 1922619) for funding.

References

1 C. A. Cantrell, R. E. Shetter and J. G. Calvert, Comparison of Perxoy Radical Concentrations at Several Contrasting Sites, *J. Atmos. Sci.*, 1995, **52**, 3408–3412.

2 Z. Tan, A. Hofzumahaus, K. Lu, S. S. Brown, F. Holland, L. G. Huey, A. Kiendler-Scharr, X. Li, X. Liu, N. Ma, K. E. Min, F. Rohrer, M. Shao, A. Wahner, Y. Wang, A. Wiedensohler, Y. Wu, Z. Wu, L. Zeng, Y. Zhang and H. Fuchs, No Evidence for a Significant Impact of Heterogeneous Chemistry on Radical Concentrations in the North China Plain in Summer 2014, *Environ. Sci. Technol.*, 2020, **54**, 5973–5979.

3 G. S. Tyndall, R. A. Cox, C. Granier, R. Lesclaux, G. K. Moortgat, M. J. Pilling, A. R. Ravishankara and T. J. Wallington, Atmospheric chemistry of small organic peroxy radicals, *J. Geophys. Res.:Atmos.*, 2001, **106**, 12157–12182.

4 A. Mellouki, T. J. Wallington and J. Chen, Atmospheric Chemistry of Oxygenated Volatile Organic Compounds: Impacts on Air Quality and Climate, *Chem. Rev.*, 2015, **115**, 3984–4014.

5 S. Y. Chen and Y. P. Lee, Transient infrared absorption of *t*-$CH_3C(O)OO$, *c*-$CH_3C(O)OO$, and α-lactone recorded in gaseous reactions of CH_3CO and O_2, *J. Chem. Phys.*, 2010, **132**, 114303.

6 M. George, M. Dolores Andrés Hernández, V. Nenakhov, Y. Liu and J. Philip Burrows, Airborne measurement of peroxy radicals using chemical amplification coupled with cavity ring-down spectroscopy: The PeRCEAS instrument, *Atmos. Meas. Tech.*, 2020, **13**, 2577–2600.

7 H. Fuchs, F. Holland and A. Hofzumahaus, Measurement of tropospheric RO_2 and HO_2 radicals by a laser-induced fluorescence instrument, *Rev. Sci. Instrum.*, 2008, **79**, 084104.

8 E. C. Wood, B. L. Deming and S. Kundu, Ethane-based chemical amplification measurement technique for atmospheric peroxy radicals, *Environ. Sci. Technol. Lett.*, 2017, **4**, 15–19.

9 S. Kundu, B. L. Deming, M. M. Lew, B. P. Bottorff, P. Rickly, P. S. Stevens, S. Dusanter, S. Sklaveniti, T. Leonardis, N. Locoge and E. C. Wood, Peroxy radical measurements by ethane-nitric oxide chemical amplification and laser-induced fluorescence during the IRRONIC field campaign in a forest in Indiana, *Atmos. Chem. Phys.*, 2019, **19**, 9563–9579.

10 J. J. Orlando and G. S. Tyndall, Laboratory studies of organic peroxy radical chemistry: An overview with emphasis on recent issues of atmospheric significance, *Chem. Soc. Rev.*, 2012, **41**, 6294–6317.

11 Z. Tan, H. Fuchs, K. Lu, A. Hofzumahaus, B. Bohn, S. Broch, H. Dong, S. Gomm, R. Häseler, L. He, F. Holland, X. Li, Y. Liu, S. Lu, F. Rohrer, M. Shao, B. Wang, M. Wang, Y. Wu, L. Zeng, Y. Zhang, A. Wahner and Y. Zhang, Radical chemistry at a rural site (Wangdu) in the North China Plain: Observation and model calculations of OH, HO_2 and RO_2 radicals, *Atmos. Chem. Phys.*, 2017, **17**, 663–690.

12 R. S. Hornbrook, J. H. Crawford, G. D. Edwards, O. Goyea, R. L. Mauldin, J. S. Olson and C. A. Cantrell, Measurements of tropospheric HO_2 and RO_2 by oxygen dilution modulation and chemical ionization mass spectrometry, *Atmos. Meas. Tech.*, 2011, **4**, 735–756.

13 M. Neumaier, R. Ruhnke, O. Kirner, H. Ziereis, G. Stratmann, C. A. M. Brenninkmeijer and A. Zahn, Impact of acetone (photo)oxidation on HO*x* production in the UT/LMS based on CARIBIC passenger aircraft observations and EMAC simulations, *Geophys. Res. Lett.*, 2014, **41**, 3289–3297.

14 S. A. McKeen, T. Gierczak, J. B. Burkholder, P. O. Wennberg, T. F. Hanisco, E. R. Keim, R.-S. Gao, S. C. Liu, A. R. Ravishankara and D. W. Fahey, The photochemistry of acetone in the upper troposphere: a source of odd-hydrogen radicals, *Geophys. Res. Lett.*, 1997, **24**, 3177–3180.

15 P. O. Wennberg, T. F. Hanisco, L. Jaeglé, D. J. Jacob, E. J. Hintsa, E. J. Lanzendorf, J. G. Anderson, R. S. Gao, E. R. Keim, S. G. Donnelly, L. A. Del Negro, D. W. Fahey, S. A. McKeen, R. J. Salawitch, C. R. Webster, R. D. May, R. L. Herman, M. H. Proffitt, J. J. Margitan, E. L. Atlas, S. M. Schauffler, F. Flocke, C. T. McElroy and T. P. Bui, Hydrogen radicals, nitrogen radicals, and the production of O_3 in the upper troposphere, *Science*, 1998, **279**, 49–53.

16 M. A. Blitz, D. E. Heard, M. J. Pilling, S. R. Arnold and M. P. Chipperfield, Pressure and temperature-dependent quantum yields for the photodissociation of acetone between 279 and 327.5 nm, *Geophys. Res. Lett.*, 2004, **31**, 1–5.

17 T. Gierczak, J. B. Burkholder, S. Bauerle and A. R. Ravishankara, Photochemistry of acetone under tropospheric conditions, *Chem. Phys.*, 1998, **231**, 229–244.

18 M. Emrich and P. Warneck, Erratum: Photodissociation of acetone in air: dependence on pressure and wavelength, behavior of the excited singlet state, *J. Phys. Chem. A*, 2000, **104**, 9436–9442.

19 A. G. Zborowska, C. Y. MacInnis, C. Z. Ye and H. D. Osthoff, On the photolysis branching ratio of methyl ethyl ketone, *Atmos. Environ.*, 2021, **254**, 118383.

20 P. R. Veres, J. M. Roberts, R. J. Wild, P. M. Edwards, S. S. Brown, T. S. Bates, P. K. Quinn, J. E. Johnson, R. J. Zamora and J. De Gouw, Peroxynitric acid (HO_2NO_2) measurements during the UBWOS 2013 and 2014 studies using iodide ion chemical ionization mass spectrometry, *Atmos. Chem. Phys.*, 2015, **15**, 8101–8114.

21 S. R. Albrecht, A. Novelli, A. Hofzumahaus, S. Kang, Y. Baker, T. Mentel, A. Wahner and H. Fuchs, Measurements of hydroperoxy radicals (HO_2) at atmospheric concentrations using bromide chemical ionisation mass spectrometry, *Atmos. Meas. Tech.*, 2019, **12**, 891–902.

22 J. Sanchez, D. J. Tanner, D. Chen, L. G. Huey and N. L. Ng, A new technique for the direct detection of HO_2 radicals using bromide chemical ionization mass spectrometry (Br-CIMS): initial characterization, *Atmos. Meas. Tech.*, 2016, **9**, 3851–3861.

23 M. F. Link, D. K. Farmer, T. Berg, F. Flocke and A. R. Ravishankara, Measuring Photodissociation Product Quantum Yields Using Chemical Ionization Mass Spectrometry: A Case Study with Ketones, *J. Phys. Chem. A*, 2021, **125**, 6836–6844.

24 S. Iyer, X. He, N. Hyttinen, T. Kurtén and M. P. Rissanen, Computational and Experimental Investigation of the Detection of HO_2 Radical and the Products of Its Reaction with Cyclohexene Ozonolysis Derived RO2 Radicals by an Iodide-Based Chemical Ionization Mass Spectrometer, *J. Phys. Chem. A*, 2017, **121**, 6778–6789.

25 M. A. Robinson, J. Andrew Neuman, L. G. Huey, J. M. Roberts, S. S. Brown and P. R. Veres, Temperature-dependent sensitivity of iodide chemical ionization mass spectrometers, *Atmos. Meas. Tech.*, 2022, **15**, 4295–4305.

26 D. L. Slusher, L. G. Huey, D. J. Tanner, F. M. Flocke and J. M. Roberts, A thermal dissociation - chemical ionization mass spectrometry (TD-CIMS) technique for the simultaneous measurement of peroxyacyl nitrates and dinitrogen pentoxide, *J. Geophys. Res.: Atmos.*, 2004, **109**, 1–13.

27 A. Hansel, W. Scholz, B. Mentler, L. Fischer and T. Berndt, Detection of RO_2 radicals and other products from cyclohexene ozonolysis with NH_4^+ and acetate chemical ionization mass spectrometry, *Atmos. Environ.*, 2018, **186**, 248–255.

28 T. Berndt, B. Mentler, W. Scholz, L. Fischer, H. Herrmann, M. Kulmala and A. Hansel, Accretion Product Formation from Ozonolysis and OH Radical Reaction of α-Pinene: Mechanistic Insight and the Influence of Isoprene and Ethylene, *Environ. Sci. Technol.*, 2018, **52**, 11069–11077.

29 A. Zaytsev, M. Breitenlechner, A. Novelli, H. Fuchs, D. A. Knopf, J. H. Kroll and F. N. Keutsch, Application of chemical derivatization techniques combined with chemical ionization mass spectrometry to detect stabilized Criegee intermediates and peroxy radicals in the gas phase, *Atmos. Meas. Tech.*, 2021, **14**, 2501–2513.

30 G. D. Edwards, C. A. Cantrell, S. Stephens, B. Hill, O. Goyea, R. E. Shetter, R. L. Mauldin, E. Kosciuch, D. J. Tanner and F. L. Eisele, Chemical Ionization Mass Spectrometer Instrument for the Measurement of Tropospheric HO_2 and RO_2, *Anal. Chem.*, 2003, **75**, 5317–5327.

31 W. Zhang and H. Zhang, Secondary Ion Chemistry Mediated by Ozone and Acidic Organic Molecules in Iodide-Adduct Chemical Ionization Mass Spectrometry, *Anal. Chem.*, 2021, 8595–8602.

32 T. H. Bertram, J. R. Kimmel, T. A. Crisp, O. S. Ryder, R. L. N. Yatavelli, J. A. Thornton, M. J. Cubison, M. Gonin, D. R. Worsnop and A. field-deployable, chemical ionization time-of-flight mass spectrometer, *Atmos. Meas. Tech.*, 2011, **4**, 1471–1479.

33 P. Brophy and D. K. Farmer, A switchable reagent ion high resolution time-of-flight chemical ionization mass spectrometer for real-time measurement of gas phase oxidized species: Characterization from the 2013 southern oxidant and aerosol study, *Atmos. Meas. Tech.*, 2015, **8**, 2945–2959.

34 F. M. Flocke, A. J. Weinheimer, A. L. Swanson, J. M. Roberts, R. Schmitt and S. Shertz, On the measurement of PANs by gas chromatography and electron capture detection, *J. Atmos. Chem.*, 2005, **52**, 19–43.

35 P. Brophy and D. K. Farmer, Clustering, methodology, and mechanistic insights into acetate chemical ionization using high-resolution time-of-flight mass spectrometry, *Atmos. Meas. Tech.*, 2016, **9**, 3969–3986.

36 J. Li, M. F. Link, S. Pandit, M. H. Webb, K. J. Mayer, L. A. Garofalo, K. L. Rediger, D. G. Poppendieck, S. M. Zimmerman, M. E. Vance, V. H. Grassian, G. C. Morrison, B. J. Turpin and D. K. Farmer, The persistence of smoke VOCs indoors: Partitioning, surface cleaning, and air cleaning in a smoke-contaminated house, *Sci. Adv.*, 2023, **9**, eadh8263.

37 I. Dotan, J. A. Davidson, G. E. Streit, D. L. Albritton and F. C. Fehsenfeld, A study of the reaction $O_3^- + CO_2 \rightleftharpoons CO_3^- + O_2$ and its implication on the thermochemistry of CO_3 and O_3 and their negative ions, *J. Chem. Phys.*, 1977, **67**, 2874–2879.

38 M. Wang, X.-C. He, H. Finkenzeller, S. Iyer, D. Chen, J. Shen, M. Simon, V. Hofbauer, J. Kirkby, J. Curtius, N. Maier, T. Kurtén, D. Worsnop, M. Kulmala, M. Rissanen, R. Volkamer, Y. J. Tham, N. Donahue and M. Sipilä, Measurement of iodine species and sulfuric acid using bromide chemical ionization mass spectrometers, *Atmos. Meas. Tech. Discuss*, 2020, 1–23.

39 L. Xu, M. M. Coggon, C. E. Stockwell, J. B. Gilman, M. A. Robinson, M. Breitenlechner, A. Lamplugh, J. D. Crounse, P. O. Wennberg, J. A. Neuman, G. A. Novak, P. R. Veres, S. S. Brown and C. Warneke, Chemical ionization mass spectrometry utilizing ammonium ions (NH_4^+ CIMS) for measurements of organic compounds in the atmosphere, *Atmos. Meas. Tech.*, 2022, **15**, 7353–7373.

40 B. Rajakumar, T. Gierczak, J. E. Flad, A. R. Ravishankara and J. B. Burkholder, The CH_3CO quantum yield in the 248 nm photolysis of acetone, methyl ethyl ketone, and biacetyl, *J. Photochem. Photobiol., A*, 2008, **199**, 336–344.

41 J. M. Mattila, P. S. J. Lakey, M. Shiraiwa, C. Wang, J. P. D. Abbatt, C. Arata, A. H. Goldstein, L. Ampollini, E. F. Katz, P. F. Decarlo, S. Zhou, T. F. Kahan, F. J. Cardoso-Saldaña, L. H. Ruiz, A. Abeleira, E. K. Boedicker, M. E. Vance and D. K. Farmer, Multiphase Chemistry Controls Inorganic Chlorinated and Nitrogenated Compounds in Indoor Air during Bleach Cleaning, *Environ. Sci. Technol.*, 2020, **54**, 1730–1739.

42 F. D. Lopez-Hilfiker, S. Iyer, C. Mohr, B. H. Lee, E. L. D'ambro, T. Kurtén and J. A. Thornton, Constraining the sensitivity of iodide adduct chemical ionization mass spectrometry to multifunctional organic molecules using the collision limit and thermodynamic stability of iodide ion adducts, *Atmos. Meas. Tech.*, 2016, **9**, 1505–1512.

43 J. D. Crounse, K. A. McKinney, A. J. Kwan and P. O. Wennberg, Measurement of gas-phase hydroperoxides by chemical ionization mass spectrometry, *Anal. Chem.*, 2006, **78**, 6726–6732.

44 L. G. Christophorou and J. K. Olthoff, Electron Interactions With Cl_2, *J. Phys. Chem. Ref. Data*, 1999, **28**, 131–169.
45 J. C. Han, M. Suto, J. C. Lee and Z. L. Petrović, Transient signals induced by laser irradiation of negative ions in hollow electrode discharges of Cl_2 and HCl in N_2, *J. Appl. Phys.*, 1990, **68**, 2649–2656.
46 L. M. Babcock and G. E. Streit, Ion–molecule reactions of Cl_2 with Cl^- and F^-, *J. Chem. Phys.*, 1982, **76**, 2407–2411.
47 B. D. Finley and E. S. Saltzman, Observations of Cl_2, Br_2, and I_2 in coastal marine air, *J. Geophys. Res.:Atmos.*, 2008, **113**, D21301.
48 W. A. Chupka, J. Berkowitz and D. Gutman, Electron affinities of halogen diatomic molecules as determined by endoergic charge transfer, *J. Chem. Phys.*, 1971, **55**, 2724–2733.
49 M. J. Travers, D. C. Cowles and G. B. Ellison, Reinvestigation of the Electron Affinities of O_2 and NO, *Chem. Phys. Lett.*, 1989, **164**, 450–455.
50 L. G. Huey, D. R. Hanson and C. J. Howard, Reactions of SF_6^- and I^- with atmospheric trace gases, *J. Phys. Chem.*, 1995, **99**, 5001–5008.
51 C. Amelynck, E. Arijs, N. Schoon and A.-M. Van Bavel, Gas phase reactions of HNO_3 with Cl^-, Cl^-H_2O, and Cl^-HCl, of Cl_2 with Cl^-H_2O and Cl^-HCl, and of HCl with Cl^-H_2O, *Int. J. Mass Spectrom.*, 1998, **181**, 113–121.
52 M. Heinritzi, M. Simon, G. Steiner, A. C. Wagner, A. Kürten, A. Hansel and J. Curtius, Characterization of the mass-dependent transmission efficiency of a CIMS, *Atmos. Meas. Tech.*, 2016, **9**, 1449–1460.
53 M. Priestley, M. Le Breton, T. J. Bannan, K. E. Leather, A. Bacak, E. Reyes-Villegas, F. De Vocht, B. M. A. Shallcross, T. Brazier, M. Anwar Khan, J. Allan, D. E. Shallcross, H. Coe and C. J. Percival, Observations of Isocyanate, Amide, Nitrate, and Nitro Compounds From an Anthropogenic Biomass Burning Event Using a ToF-CIMS, *J. Geophys. Res.:Atmos.*, 2018, **123**, 7687–7704.